Novel Statistical Analysis Schemes for Frequency-Modulated Thermal Wave Imaging for Inspection of Ship Hull Materials

Ishant Singh [1], Vanita Arora [2], Prabhu Babu [3] and Ravibabu Mulaveesala [1,*]

[1] InfraRed Imaging Laboratory (IRIL), Centre for Sensors, Instrumentation and Cyber Physical System Engineering (SeNSE), Indian Institute of Technology Delhi, Hauz Khas, New Delhi 110016, India
[2] InfraRed Vision & Automation Pvt. Ltd., Sun City, Rupnagar 140001, India
[3] Centre for Applied Research in Electronics (CARE), Indian Institute of Technology Delhi, Hauz Khas, New Delhi 110016, India
* Correspondence: mulaveesala@sense.iitd.ac.in

Abstract: In the field of thermal non-destructive testing and evaluation (TNDT&E), active thermography gained popularity due to its fast wide-area monitoring and remote inspection capability to assess materials without compromising their future usability. Among the various active thermographic methods, pulse compression-favorable frequency-modulated thermal wave imaging stands out for its enhanced detectability and depth resolution. In this study, an experimental investigation has been carried out on a hardened steel sample used in the ship building industry with a flat-bottom-hole-simulated defect using the frequency-modulated thermal wave imaging (FMTWI) technique. The defect detection capabilities of FMTWI have been investigated from various statistical post-processing approaches and compared by taking the signal-to-noise ratio (SNR) as a figure of merit. Among various adopted statistical post-processing techniques, pulse compression has been carried out using different methods, namely the offset removal with polynomial curve fitting and principal component analysis (PCA), which is an unsupervised learning approach for data reduction and offset removal with median centering for data standardization. The performance of these techniques was assessed through experimental investigations on hardened steel specimens used in ship building to provide valuable insights into their effectiveness in defect detection capabilities.

Keywords: non-destructive testing and evaluation; frequency-modulated thermal wave imaging; principal component analysis; pulse compression; principal component thermography

1. Introduction

Non-destructive testing and evaluation (NDT&E) approaches, especially thermal non-destructive testing, are becoming increasingly common for detecting the presence of underlying faults in a material being inspected without affecting its output or functionality [1]. Three widely used active NDT&E procedures in the industry are pulse thermography (PT), lock-in thermography (LT), and pulse phase thermography (PPT) [2,3]. In PT, the surface of the test material becomes heated from a short pulse of high peak power. Data are acquired while the sample cools down and are later analyzed. But the method is not as efficient because of uneven surface heating due to changes in emissivity [4]. So, to address this limitation, LT was developed. LT solves this issue by using a periodic sinusoidal thermal wave with lower peak power for a longer duration [5]. This method is less likely to be affected by temperature noise because phase images are used instead of magnitude images during analysis [6]. The primary drawback with this technique is that it needs to be performed multiple times at different frequencies for respective depths, which makes testing time-consuming. To tackle the issue of surface temperature variation and long experimentation times, PPT was introduced; it combines the best parts of both PT and LT into a single method [7]. Using just pulse stimulation makes it better for finding deeper flaws and eliminates the effects of surface temperature variation as the data are

analyzed in phase analyses, but the issue of a high peak power requirement still prevails. To overcome the limitations of conventional techniques, new advanced thermographic excitation techniques were introduced. These recent advances in TNDT&E methods include pulse compression favorable excitation techniques to overcome the limitations of traditional techniques [8]. These techniques have become popular because they offer high sensitivity and precision for finding defects and detecting them at different depths below the surface. Frequency-modulated thermal wave imaging (FMTWI) methods are used in this study. This technique uses a linearly modulated band of frequencies that gives better contrast and depth resolution based on the specimen's thermal diffusivity and size [9]. So, this eliminates the requirement for high peak power or a long testing time. This lets us cover different depths in a single run of the experiment. Previous studies on steel materials primarily focused on conventional techniques such as LT and PPT [10,11], with some testing conducted on mild steel samples using frequency-modulated thermography, which improved the SNR and presented better depth penetration. In contrast, this work explores subsurface defects in hardened steel samples used in ship building applications using FMTWI.

The data captured with an infrared camera are stored in the form of a 3D matrix which consists of a thermographic sequence. The data are then enhanced with different post-processing techniques, i.e., pulse compression, which is a signal processing technique that concentrates most of the signal power in the central lobe, thus improving range resolution and the signal-to-noise ratio [12] and PCA (with different standardization approaches), which is a multivariate data processing technique that reduces the dimensions of large data to the principal components that retain most variance [13]. This work has compared the mentioned statistical post-processing approaches on data acquired with FMTWI on their capability of effectively preserving defect shape and contrast and the SNR as figure of merit on a hardened steel specimen with a flat bottom hole.

2. Theory

A linear frequency-modulated thermal wave with a frequency range of 0.01 Hz to 0.1 Hz is applied to the material for 100 s during FMTWI excitation, which provides improved depth resolution [14]. Thus, a heatwave is generated with help of halogen lamps in the experimentation following FMTWI excitation, which is captured with an infrared camera. The applied heatwave penetrates the test material, leading to a temperature change on the surface. Underlying defects cause a temperature gradient because of variations in emissivity, which the one-dimensional Fourier's diffusion equation may theoretically explain [15].

$$\frac{\partial^2 T(x,t)}{\partial x^2} = \frac{1}{\alpha} \frac{\partial T(x,t)}{\partial t} \tag{1}$$

Thermal diffusivity is represented by α. To find the surface temperature for the following boundary condition in a slab of thickness L, Equation (1) is solved in the Laplace domain as follows:

$$\check{T}(x,s) = \frac{Q(s)}{k\sigma(1 - e^{-2\sigma L})} \left[e^{-\sigma x} + e^{\sigma(x-2L)} \right] - \frac{T_0}{s} \tag{2}$$

where $\sigma = \sqrt{\frac{s}{\alpha}}$.

Consequently, this can be inferred from the foregoing equations that the frequency at any given time determines the depth resolution over time. Consequently, depth resolution with time-varying instantaneous frequency is provided by time-varying chirp waves [16].

Several post-processing techniques are used to precisely identify underlying defects in a hardened steel material that has been exposed to external excitation, which results in heat distribution over its surface. These methods seek to decrease data dimensionality, increase sensitivity, and improve flaw detectability.

Pulse compression: With this method, the thermographic data that are recorded during active heating and subsequently offset are removed using first-order polynomial curve fitting on the FMTWI data [17]. Further pulse-compressed thermal images are reconstructed. The approach of pulse compression involves calculating the cross-correlation (*CC*) between the offset-removed signal at the defect-free sound region and the signal of each pixel [18–20].

$$CC(\tau) = P(t) \bigotimes R(t + \tau) \tag{3}$$

$$CC(\tau) = \int_{-\infty}^{+\infty} P(t) * R(t + \tau) dt \tag{4}$$

Here, *P(t)* is the offset-removed signal at various locations in the test sample and *R(t)* is the reference signal. The cross-correlation of two signals is represented in Equations (3) and (4), where *t* and τ stand for time and time delay, respectively [21]. The main advantage of pulse compression is that it concentrates all the energy into a shorter amount of time, which improves the signal-to-noise ratio (SNR) and depth resolution [22].

Principal component thermography: An advanced data processing method called principal component thermography (PCT) is applied in thermographic inspection to improve the identification of material defects [23]. By using principal component analysis (PCA) on thermographic data, this technique enhances thermal gradients and anomalies that can point to the presence of defects [24]. PCA is a type of multivariate data analysis that is used for a more efficient processing of higher dimensional data. Principal components (PCs), which are uncorrelated vectors arranged in decreasing variance order, are the result of this transformation of the data [25], which are then projected onto the standardized data and reconstructed using the selected number of PCs; typically, the first few PCs contain the majority of variance and allow for a relatively loss-free reconstruction of the data [26]. In this work, the approach used is median centering, as a novel approach for data standardization, and it was compared with conventional mean-centered results.

The obtained experimental thermographic data are a three-dimensional matrix with a size of M × N × T, where T is the number of experimental frames and M × N is the spatial resolution of the data taken with an infrared camera. First, data are converted from a 3D matrix to a 2D matrix, i.e., *W* of dimension P × T, where P is the product of M and N, to use PCA for data reduction. As a result, each row in matrix *W* represents a capture frame's features and elements.

$$W_{std} = W - W_{median/mean} \tag{5}$$

The standardized matrix in Equation (5), denoted as W_{std}, is obtained by subtracting $W_{median/mean}$ from the W matrix. PCA is applied using eigenvalue decomposition (EVD) on the covariance matrix W_{std} [27].

$$W_{cov} = \frac{W_{std} * W_{std}^T}{N - 1} \tag{6}$$

In Equation (6), W_{cov} is covariance matrix of W_{std}.

$$W_{cov} = VSV^T \tag{7}$$

In Equation (7), *S* is a singular matrix with all the eigenvalues arranged in descending order and *V* is an orthogonal matrix [28]. The coefficients of principle components (PCs) are stored in matrix *V* in descending order of variance. The standardized data are then multiplied by the coefficient matrix of the PC vector after selecting P number of PCs.

$$V_P = V_{NX1} \tag{8}$$

$$W_{pc} = W_{std} * V_P \tag{9}$$

$$W_{reconstructed} = W_{pc} * V_P^T \tag{10}$$

From Equations (8) and (9), V_P is the Pth PC vector of V matrix and W_{pc} is the Pth principal component constructed by projecting V_P onto the standardized data [29]. Reconstructing the data of the subsequent PCs is performed by multiplying the transpose of V_P to the calculated principal component, i.e., $W_{reconstructed}$, as shown in Equation (10). Furthermore, the data are converted back to a 3D matrix.

The post-processing approach utilized is illustrated in Figure 1.
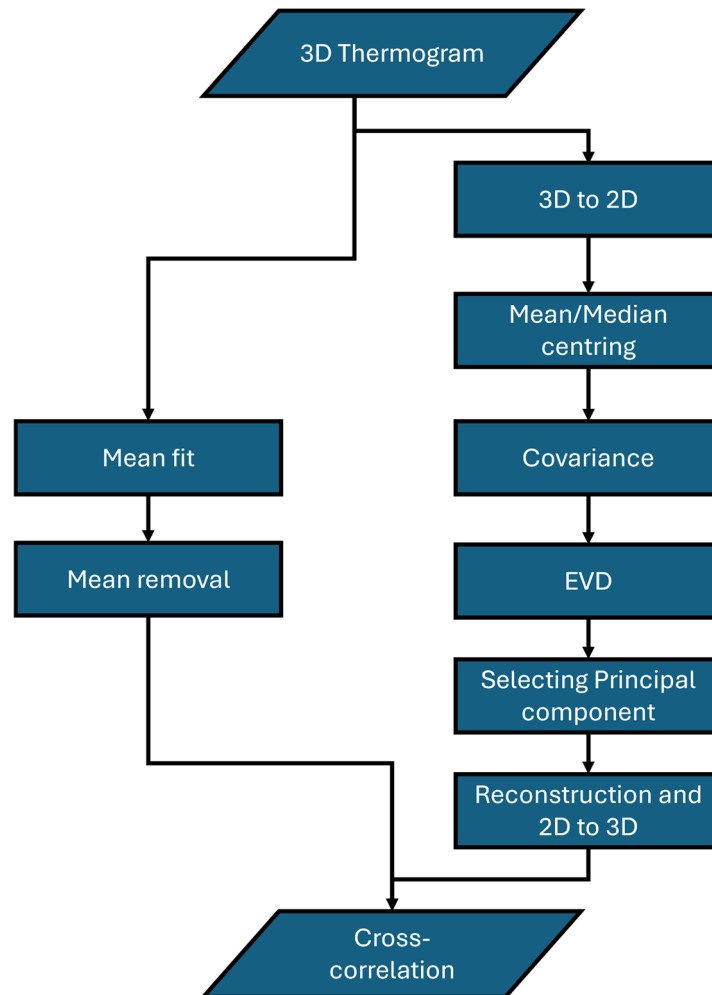
Figure 1. Flow diagram for cross-correlation-based pulse compression with mean removal and PCA.

3. Experimentation and Test Sample

The sample used in the experimentation was hardened steel used in ship building with a 6 mm thickness and a cross-section of 75 mm × 75 mm, consisting of 1 flat bottom hole of a radius of 28 mm at a depth of 2 mm, as shown in Figure 2. Figure 3 shows the experimental setup used for acquiring the data; two halogen lamps were used to excite the data, which deliver a power of 1 kW each, and the sample was kept at a distance of 1 m from the lamps for uniform illumination. The intensity of the lamp was controlled by a source control unit with intensity varying by following the FMTWI modality with frequency varying from 0.01 Hz to 0.1 Hz for 100 s [30]. The source control unit and interfacing along with analysis software is developed by the InfraRed Vision & Automation Pvt. Ltd., Rupnagar, Punjab, India whereas the infrared camera (FLIR-A655sc with a spatial resolution of 640 × 480, a spectral sensitivity of 7 μm to 14 μm, a frame rate up to 50 fps, a standard temperature range of −40 °C to 650 °C, and a temperature sensitivity of 30 mK) is procured from Sweden. Which was used to record temporal temperature

distribution over the sample at a frame rate of 25 frames per second (fps) during the active frequency-modulated thermal excitation.
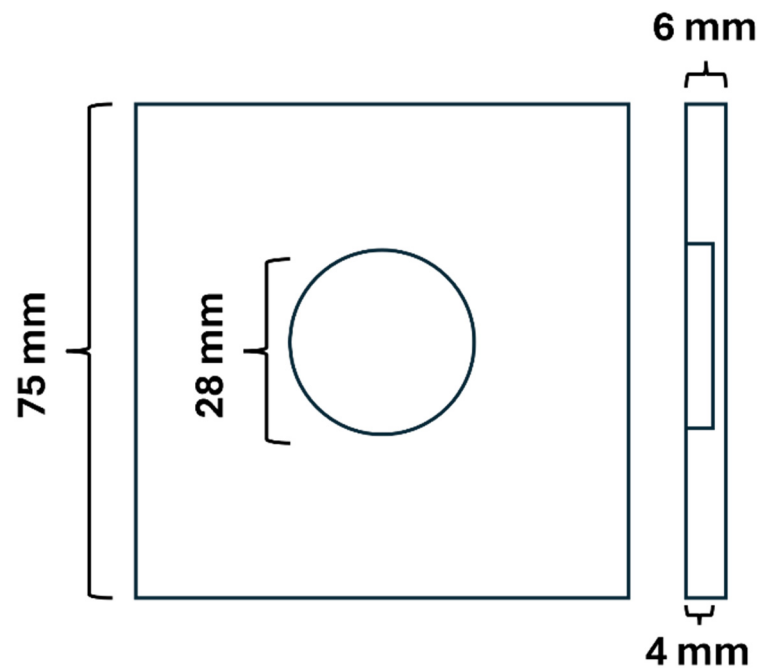
Figure 2. Schematic for hardened steel sample with flat bottom hole at center.

Figure 3. Illustration of the experimental setup used for FMTWI.

4. Results and Discussion

For the quantitative analysis and comparison of different post-processing techniques, the SNR at the defect location is calculated as figure of merit. The following approach is

suitable for this work because different post-processing schemes are compared. The SNR is calculated as [31]

$$SNR(dB) = 20 * log_{10} \frac{\mu_{def} - \mu_h}{\sigma_{def} - \sigma_h} \tag{11}$$

In Equation (11) above, μ_{def} and σ_{def} are the mean and standard deviation of the pixel region at the defect location, μ_h and σ_h are the mean and standard deviation at a healthy or non-defective region.

The next processing step performed is pulse compression on the thermographic data. Figure 4 shows the thermal profile and the offset-removed thermal profile along the frames for a defective and healthy region, and respective best correlation images obtained along the correlation profile are shown in Figure 4.

(a)　　　(b)
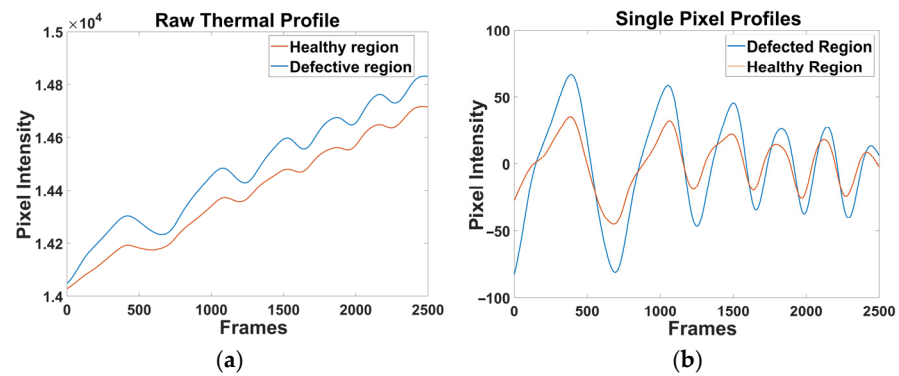
Figure 4. Illustrated (**a**) raw temporal response and (**b**) offset-removed profile for FMTWI from 0.01 Hz to 0.1 Hz.

Here, in Figure 5, it is visible that pulse compression has an excellent contrast for the specimen used in this experiment. Further on in this work, pulse compression is implemented with PCA and compared to the results with polynomial curve fitting.

(a)　　　(b)
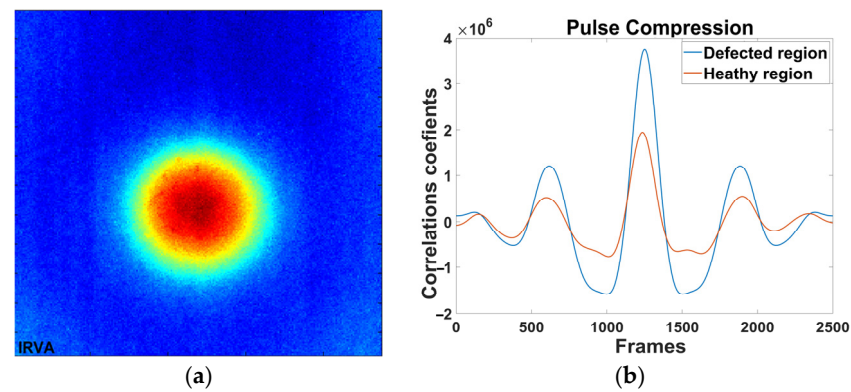
Figure 5. Reconstructed pulse-compressed (**a**) spatial thermal distribution and (**b**) correlation coefficients of offset-removed temporal response for healthy and defective location.

Further on in the work, principal component thermography (PCT) with median centering for standardization is conducted. PCT decomposed data into different principal components (PCs) in order of decreasing variance. Thus, mean centering and median centering are compared for standardization. The thermographic data were standardized using two different methods, namely the mean removal and median removal. The data were then reconstructed using the first three principal components (PC1, PC2, and PC3).

As Figures 6–8 show, the thermal profile in PC1 exhibited the most variance and closely resembled the original thermal profile for both standardization methods. This indicates that most of the relevant thermal information is captured in PC1. PC2, for both mean-removed

and median-removed data, showed similar characteristics to an offset-removed profile. PC2 also provided the best contrast, making it useful for highlighting variations that are not as prominent in PC1.
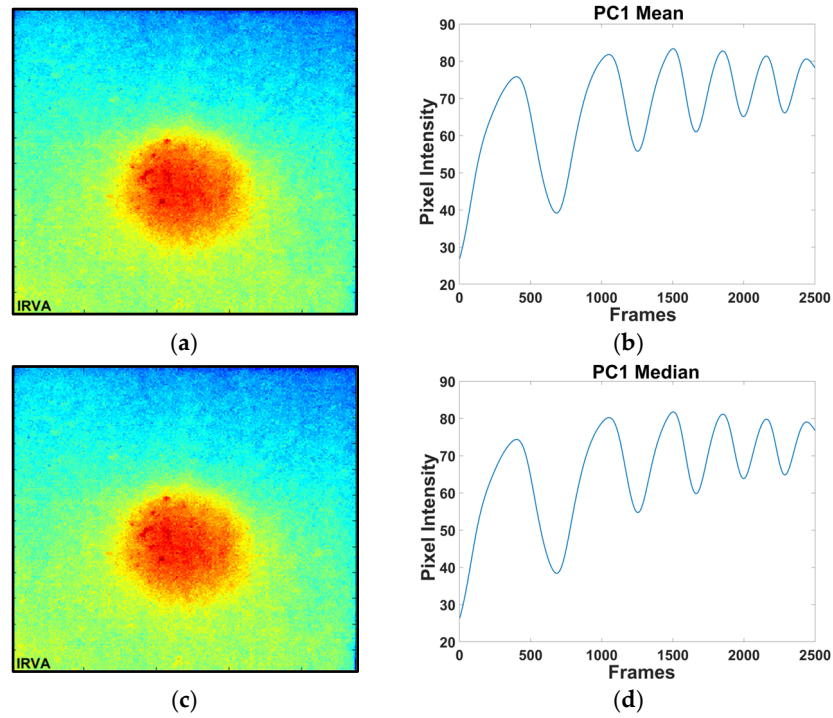
Figure 6. Reconstructed (**a**,**b**) spatial thermal distribution and (**c**,**d**) temporal response obtained from PC1 for mean and median centering, respectively.
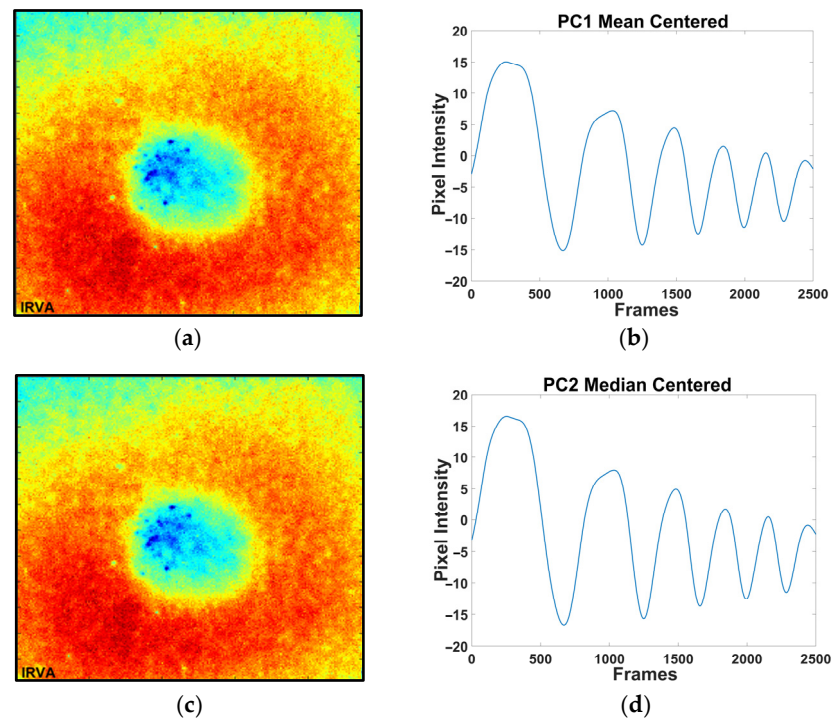
Figure 7. Reconstructed (**a**,**b**) spatial thermal distribution and (**c**,**d**) temporal response obtained from PC2 for mean and median centering, respectively.
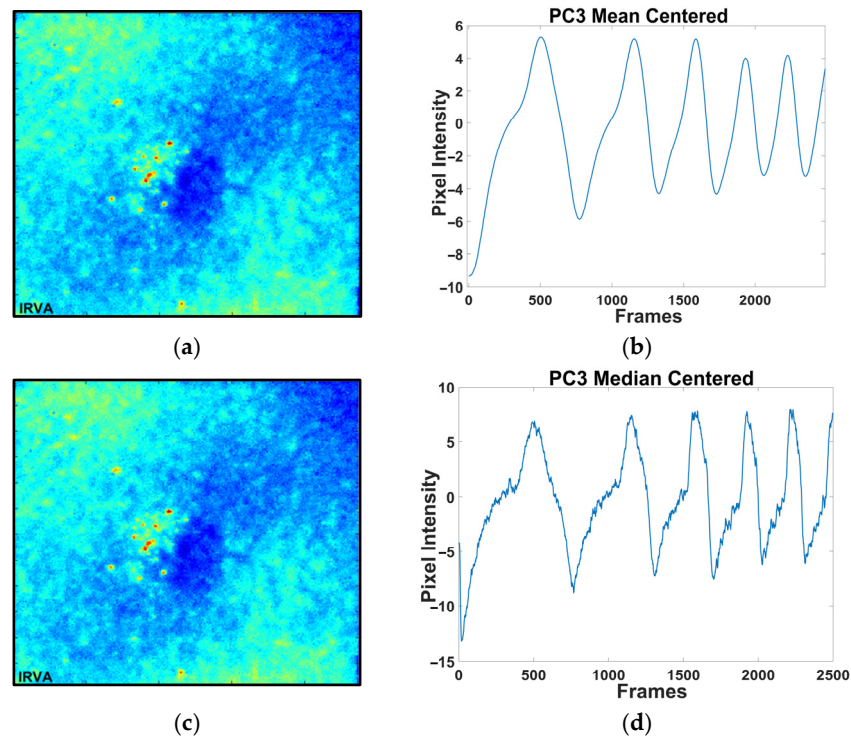
Figure 8. Reconstructed (**a**,**b**) spatial thermal distribution and (**c**,**d**) temporal response obtained from PC3 for mean and median centering, respectively.

The thermal profiles in PC3 began to lose their shape and the signal quality diminished. This suggests that PC3 captures less relevant information and introduces noise into the thermal profile, especially in the median-removed profile. When comparing the contrast, PC2 provided the best contrast, effectively highlighting features in the hardened steel sample. In contrast, PC3 failed to provide any meaningful contrast, indicating that it does not contribute significantly to the detection of thermal anomalies.

The resolution in PC1 and PC2 was sufficient to capture major defects, but PC3's loss of detail in temporal resolution indicates a drop in accuracy. Thus, the pulse compression of PC2 enhanced resolution and accuracy. So, a further comparison of pulse compression of mean- and median-centered data for PC2 is shown in Figure 9.
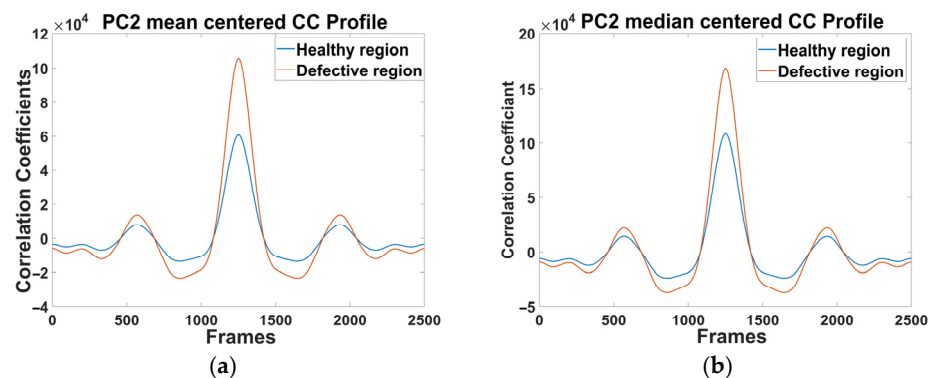
Figure 9. Cross-correlation profile for (**a**) mean-centered and (**b**) median-centered PC2 thermal profile.

Figure 9 shows correlation for PC2 on both mean-centered and median-centered data and on this sample, it can be observed that median centering provides a better peak-to-side lobe ratio, which means a better suppression of noise in the compressed pulse. However, when comparing enhanced contrast, both techniques have similar performance (Figure 10). From Figures 5b and 9, PCT provides a better peak-to-side ratio than pulse

compression with polynomial curve fitting. Comparing contrasts, the polynomial curve fit has the highest contrast but PCT captures the thermal gradient over the material surface more efficiently.

(**a**)   (**b**)
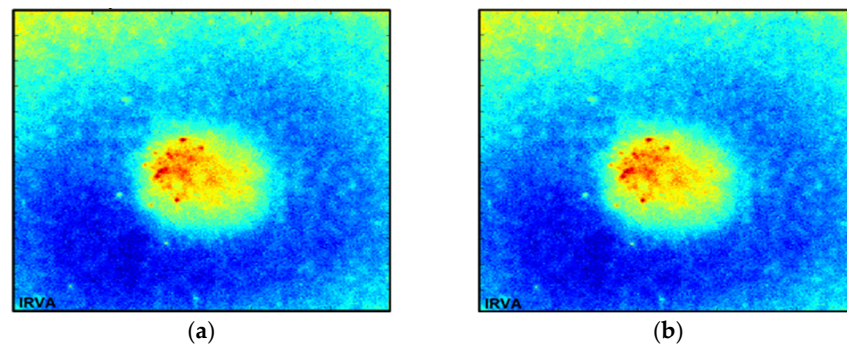
Figure 10. Illustrated reconstructed spatial thermal distribution obtained by pulse compression of (**a**) mean-centered and (**b**) median-centered PC2 signal.

Furthermore, for comparing all the techniques, results have been evaluated taking the SNR as figure of merit, as in Equation (11); thus, results show that pulse compression (CC) has the highest SNR, followed by PC2 with pulse compression, then PC2 and PC1 for both mean and median centering, both having a similar contrast and SNR for both mean and median centering.

Thus, different methods are compared, as shown in Table 1. It was observed that PCA as preprocessing reduces the data effectively, i.e., it makes data processing much more efficient among all the techniques with a high signal-to-noise ratio.

Table 1. SNR values for various post-processing techniques.

Post-Processing Technique	SNR in dB
CC	34.304
PC1 MEAN	26.512
PC1 MEDIAN	26.512
PC2 MEAN	27.724
PC2 MEDIAN	27.724
PC2 MEAN CC	33.676
PC2 MEDIAN CC	33.676

5. Conclusions

This paper examines the effectiveness of various statistical post-processing techniques for detecting defects in hardened steel used in ship building using frequency-modulated thermal wave imaging. Experimental findings indicate that for contrast evaluation, pulse compression with polynomial curve fitting as preprocessing outperforms other methods. Additionally, PCA with either mean or median centering shows a similar performance on hardened steel specimens. The advantage of PCA lies in its superior performance in data dimensionality reduction, as shown in Figures 5b and 9. While pulse compression yields the highest SNR, integrating PCA as a preprocessing step for pulse compression, though slightly reducing the SNR compared to the conventional pulse compression technique, significantly speeds up processing due to the substantial reduction in data dimensions, as illustrated in Figures 4b and 7b,d. Pulse compression with PCA achieves better contrast and detectability than conventional PCA. Furthermore, in terms of the signal-to-noise ratio (SNR), pulse compression achieves the highest SNR, followed by pulse compression with PCA giving similar results for both mean- and median-centered data, followed by PC2

and PC1 for both mean and median centering. PC3 results fail to detect the defect and the signal starts to lose information, thus discarding it for further comparison.

Author Contributions: I.S. contributed to writing the manuscript and experimentation along with algorithm development; V.A. contributed in developing the software for control heat sources and analysis software; P.B. contributed by reviewing the work and providing the suggestions; R.M. overall management, sample preparation and suggestions. All authors have read and agreed to the published version of the manuscript.

Institutional Review Board Statement: Not applicable.

Informed Consent Statement: Not applicable.

Data Availability Statement: No data generated from the experiments presented in this manuscript.

Conflicts of Interest: Vanita Arora was employed by the InfraRed Vision & Automation Pvt. Ltd. The remaining authors declare that the research was conducted in the absence of any commercial or financial relationships that could be construed as a potential conflict of interest.

References

1. Maldague, X. *Theory and Practice of Infrared Technology for Nondestructive Testing*; John Wiley & Sons: Hoboken, NJ, USA, 2001.
2. Maldague, X.P.V. Introduction to NDT by active infrared thermography. *Mater. Eval.* **2002**, *60*, 1060–1073.
3. Yang, R.; He, Y. Optically and non-optically excited thermography for composites: A review. *Infrared Phys. Technol.* **2016**, *75*, 26–50. [CrossRef]
4. Jena, C.; Sarbhai, N.; Mulaveesala, R.; Tuli, S. Pulsed Thermography Simulation: 1D, 2D and 3D Electro-Thermal Model Based Evaluation. Available online: https://www.ndt.net/?id=4376 (accessed on 10 October 2024).
5. Montanini, R. Quantitative determination of subsurface defects in a reference specimen made of Plexiglas by means of lock-in and pulse phase infrared thermography. *Infrared Phys. Technol.* **2010**, *53*, 363–371. [CrossRef]
6. Chernykh, S.E.; Kostin, V.N.; Komolikov, Y.I. Thermal Testing of Corundum Ceramic Plates. *Russ. J. Nondestruct. Test.* **2023**, *59*, 977–984. [CrossRef]
7. Maldague, X.; Marinetti, S. Pulse phase infrared thermography. *J. Appl. Phys.* **1996**, *79*, 2694–2698. [CrossRef]
8. Mulaveesala, R.; Dua, G.; Arora, V.; Siddiqui, J.A.; Muniyappa, A. Pulse compression favourable aperiodic infrared imaging approach for non-destructive testing and evaluation of bio-materials. In *Thermosense: Thermal Infrared Applications XXXIX*; SPIE: Bellingham, WA, USA, 2017; p. 102140G. [CrossRef]
9. Tuli, S.; Chatterjee, K. Frequency modulated thermal wave imaging. *AIP Conf. Proc.* **2012**, *1430*, 523–526. [CrossRef]
10. Krapez, J.-C.; Pacou, D.; Gardette, G. Lock-in thermography and fatigue limit of metals. In Proceedings of the 2000 International Conference on Quantitative InfraRed Thermography, QIRT Council, 2000, Reims, France, 18–21 July 2000. [CrossRef]
11. Chung, Y.; Shrestha, R.; Lee, S.; Kim, W. Thermographic Inspection of Internal Defects in Steel Structures: Analysis of Signal Processing Techniques in Pulsed Thermography. *Sensors* **2020**, *20*, 6015. [CrossRef]
12. Silipigni, G.; Burrascano, P.; Hutchins, D.A.; Laureti, S.; Petrucci, R.; Senni, L.; Torre, L.; Ricci, M. Optimization of the pulse-compression technique applied to the infrared thermography nondestructive evaluation. *NDT E Int.* **2017**, *87*, 100–110. [CrossRef]
13. Vavilov, V.P.; Chulkov, A.O.; Shiryaev, V.V.; Kuimova, M.V.; Zhang, H. Noise suppression in pulsed IR thermographic NDT: Efficiency of data processing algorithms. *NDT E Int.* **2024**, *148*, 103240. [CrossRef]
14. Mulaveesala, R.; Arora, V.; Dua, G.; Rani, A.; Kher, V.; Sharma, A.; Kaur, K. Pulse compression favorable thermal wave imaging methods for testing and evaluation of carbon fibre reinforced polymer. *SPIE-Intl. Soc. Opt. Eng.* **2020**, *11409*, 114090S. [CrossRef]
15. Sharma, A.; Mulaveesala, R.; Arora, V. Novel Analytical Approach for Estimation of Thermal Diffusivity and Effusivity for Detection of Osteoporosis. *IEEE Sens. J.* **2020**, *20*, 6046–6054. [CrossRef]
16. Mulaveesala, R.; Ghali, V.S.; Arora, V. Applications of non-stationary thermal wave imaging methods for characterisation of fibre-reinforced plastic materials. *Electron. Lett.* **2013**, *49*, 118–119. [CrossRef]
17. Mulaveesala, R.; Vaddi, J.S.; Singh, P. Pulse compression approach to infrared nondestructive characterization. *Rev. Sci. Instrum.* **2008**, *79*, 9. [CrossRef]
18. Tabatabaei, N.; Mandelis, A.; Amaechi, B.T. Thermophotonic radar imaging: An emissivity-normalized modality with advantages over phase lock-in thermography. *Appl. Phys. Lett.* **2011**, *98*, 163706. [CrossRef]
19. Tabatabaei, N. Matched-Filter Thermography. *Appl. Sci.* **2018**, *8*, 581. [CrossRef]
20. Ricci, M.; Zito, R.; Laureti, S. Pseudo-noise pulse-compression thermography: A powerful tool for time-domain thermography analysis. *NDT E Int.* **2024**, *148*, 103218. [CrossRef]
21. Gong, J.; Liu, J.; Qin, L.; Wang, Y. Investigation of carbon fiber reinforced polymer (CFRP) sheet with subsurface defects inspection using thermal-wave radar imaging (TWRI) based on the multi-transform technique. *NDT E Int.* **2014**, *62*, 130–136. [CrossRef]

22. Dua, G.; Arora, V.; Mulaveesala, R. Defect Detection Capabilities of Pulse Compression Based Infrared Non-Destructive Testing and Evaluation. *IEEE Sens. J.* **2021**, *21*, 7940–7947. [CrossRef]
23. Rajic, N. Principal component thermography for flaw contrast enhancement and flaw depth characterisation in composite structures. *Compos. Struct.* **2002**, *58*, 521–528. [CrossRef]
24. Yousefi, B.; Sfarra, S.; Sarasini, F.; Castanedo, C.I.; Maldague, X.P.V. Low-rank sparse principal component thermography (sparse-PCT): Comparative assessment on detection of subsurface defects. *Infrared Phys. Technol.* **2019**, *98*, 278–284. [CrossRef]
25. Marinetti, S.; Grinzato, E.; Bison, P.; Bozzi, E.; Chimenti, M.; Pieri, G.; Salvetti, O. Statistical analysis of IR thermographic sequences by PCA. *Infrared Phys. Technol.* **2004**, *46*, 85–91. [CrossRef]
26. Das, P.; Arora, V.; Mulaveesala, R. Novel Insights on Spatio-Temporal Analysis for Frequency Modulated Thermal Wave Imaging Using Principal Component Analysis on Glass Fibre Reinforced Polymer Material. *J. Nondestruct. Eval.* **2024**, *43*, 34. [CrossRef]
27. Ibarra-Castanedo, C.; González, D.; Klein, M.; Pilla, M.; Vallerand, S.; Maldague, X. Infrared image processing and data analysis. *Infrared Phys. Technol.* **2004**, *46*, 75–83. [CrossRef]
28. Ebrahimi, S.; Fleuret, J.; Klein, M.; Théroux, L.-D.; Georges, M.; Ibarra-Castanedo, C.; Maldague, X. Robust Principal Component Thermography for Defect Detection in Composites. *Sensors* **2021**, *21*, 2682. [CrossRef]
29. Milovanović, B.; Gaši, M.; Gumbarević, S. Principal Component Thermography for Defect Detection in Concrete. *Sensors* **2020**, *20*, 3891. [CrossRef] [PubMed]
30. Ghali, V.S.; Mulaveesala, R. Frequency modulated thermal wave imaging techniques for non-destructive testing. *Insight Non-Destruct. Test. Cond. Monit.* **2010**, *52*, 475–480. [CrossRef]
31. Kaur, K.; Mulaveesala, R. An efficient data processing approach for frequency modulated thermal wave imaging for inspection of steel material. *Infrared Phys. Technol.* **2019**, *103*, 103083. [CrossRef]